Effect of thermodenuding on the structure of nascent flame soot aggregates

Janarjan Bhandari[1], Swarup China[1,*], Timothy Onasch[2,3], Lindsay Wolff[3], Andrew Lambe[2,3], Paul Davidovits[3], Eben Cross[2], Adam Ahern[4], Jason Olfert[5], Manvendra Dubey[6], Claudio Mazzoleni[1]

[1]Department of Physics and Atmospheric Sciences Program, Michigan Technological University, Houghton, MI, 49931, USA
[2]Aerodyne Research Inc., Billerica, MA, 01821, USA
[3]Chemistry Department, Boston College, Chestnut Hill, MA, 02467, USA
[4]Centre for Atmospheric Particle Studies, Carnegie Mellon University, Pittsburgh, PA, 15232, USA
[5]Department of Mechanical Engineering, University of Alberta, Edmonton, Alberta, T6G 2G8, Canada
[6]Earth and Environmental Sciences Division, Los Alamos National Laboratory, Los Alamos, NM, 87545, USA
[*] Now at: Pacific Northwest National Laboratory, Richland, WA, 99354, USA

Abstract. The optical properties (light scattering and absorption) of soot particles depend on soot size and index of refraction, but also on the soot complex morphology and the internal mixing with other material at the single particle level. For example, freshly emitted (nascent) soot particles can interact with other materials in the atmosphere, materials that can condense on soot and coat it. This coating can affect the soot optical properties by refracting light, or by changing the soot aggregate structure. A common approach to studying the effect of coating on soot optical properties is to measure absorption and scattering values in ambient air and then measure them again after removing the coating using a thermodenuder. In this approach, it is assumed that: 1) Most of the coating material is removed; 2) charred organic coating does not add to the refractory carbon; 3) oxidation of soot is negligible; and 4) the pre-existing core soot structure is left unaltered despite potential oxidation of the core at elevated temperatures. In this study, we investigate the validity of the last assumption, by studying the effect of thermodenuding on the morphology of nascent soot. To this end, we analyze the morphological properties of laboratory generated nascent soot, before and after thermodenuding. Our investigation shows that there is only minor restructuring of nascent soot by thermodenuding.

1 Introduction

Soot particles are mostly composed of refractory carbonaceous material that forms from incomplete combustion during burning activities (Haynes and Wagner, 1981). A nascent soot particle appears as a fractal-like (sometimes referred to as a lacy) aggregate of small spherules (called nanospheres or monomers) (Buseck et al., 2014) and its structure is scale invariant (Sorensen, 2001). Here, the term nascent is used to refer to freshly emitted soot particles that have negligible coating on the nanospheres. The diameter of these nanospheres varies in a range from 10 nm to more than 50 nm depending on the fuel source and combustion conditions (e.g., Adachi and Buseck, 2008; Bambha et al., 2013b; China et al., 2014; Park et al., 2004). During atmospheric processing, soot particles interact with organic and inorganic materials (in the form of aerosol or condensable vapors). During these interactions, soot undergoes morphological changes including for example compaction, coagulation and coating (e.g., China et al., 2015b). Even in very controlled combustions, and depending upon the flaming conditions and fuel types, it is common for

combustion generated soot aggregates to have different kinds of polycyclic aromatic hydrocarbons (PAHs) thinly coating the monomers (Cross et al., 2010). In this case, coating is acquired at the source, not added later through atmospheric processing. Coating or internal mixing in general, changes the optical properties of soot even when the structure of the refractory components remains the same. These changes consequently affect the radiative forcing of soot (e.g., Adachi and Buseck, 2013; Ghazi and Olfert, 2013; Jacobson, 2001; Lack and Cappa, 2010; Liu et al., 2015a; Schnitzler et al., 2014; Van Poppel et al., 2005; Westcott et al., 2008). Several studies have also shown that coating of soot by partially-absorbing or non-absorbing materials increases the absorption and scattering cross sections (Cappa et al., 2012; Fuller et al., 1999; Khalizov et al., 2009; Lack and Cappa, 2010; Liu et al., 2015b). These increases are termed as absorption and scattering enhancements (E_{abs} and E_{sca}). The enhancement is typically calculated as the ratio of the light absorption or scattering coefficient of the coated soot to the light absorption or scattering coefficient of the soot after the coating material has been removed (Lack and Cappa, 2010).

Thermodenuders (TDs) that remove the coating by evaporation are often used in the field and in the laboratory to study and quantify these optical enhancements (Bambha et al., 2013b; Ghazi and Olfert, 2013; Lack et al., 2012; Xue et al., 2009). During the thermodenuding process, coated soot particles are passed through a heated column, typically at ~200-300 ºC to evaporate volatile coating material while leaving behind the refractory soot (Huffman et al., 2008; Wehner et al., 2002). The temperature gradient within the TD can result in particle losses due to thermophoretic forces, though these losses can be measured and accounted for (Huffman et al., 2008). To correctly assess the E_{abs} and E_{sca} using a TD, one needs to make the following assumptions: 1) Most of the coating materials is removed from the soot by the TD; 2) organic coating material does not transform into refractory carbon due to charring; 3) refractory carbon is not oxidized to a substantial extent under the elevated temperature; and 4) the structure of the refractory soot particle is unaffected, meaning that the thermodenuding process alone does not induce restructuring of the lacy soot aggregates.

Contrary to assumption 1), the thermodenuding may not remove refractory particulate material, such as some inorganic salts from soot particle and may not remove all of the non-refractory material (Cappa et al., 2013). For example, Liu et al. (2015b) observed that denuded soot still contained heavily coated soot particles although in smaller fraction, suggesting that the TD may not remove the coating completely, especially for ambient samples. Healy et al. (2015) found that on average only 74% of the mass of coating material was removed from soot samples after thermodenuding. The mass removal efficiency by the TD was even less (approximately 60%) for wildfire emission samples. Swanson and Kittelson (2010) have also cautioned about semi-volatile particle artifacts due to incomplete removal of evaporated compounds in the TD. Similarly, Knox et al. (2009) found that there was no significant difference in the mass absorption cross section between the themodenuded and non-thermodenuded aged-soot sample compared to fresh soot, due to the incomplete removal of coating materials from aged soot particles. On the other hand, Khalizov et al. (2013) hypothesize that the thermodenuder may remove all of the coating material from ambient soot, including the coating acquired during atmospheric processing as well as the nascent coating present on soot at the source, and therefore, they suggest that the denuded particles cannot represent the nascent soot morphology.

Next we briefly discuss the assumptions 2) and 3). The elevated temperatures during the thermodenuding process may cause charring of some organic matter into refractory, elemental carbon and /or some oxidation of the carbonaceous matter. Charring of organic particulate material into elemental carbon is a known phenomenon under the elevated temperature in OCEC techniques (Chow et al., 2004; Countess, 1990). Issues that influence charring include temperatures and residence times, as well as chemical composition. Charring is likely more of an issue for oxidized organics, such as biomass burning or SOA, than reduced organics, such as efficient combustion products (i.e., diesel and laboratory flame soot) (Cheng et al., 2011; Khan et al., 2012). Two significant differences between OCEC and thermodenuding include: (1) OCEC techniques typically operates at higher temperatures than TDs, and (2) OCEC charring occurs in a helium atmosphere, whereas thermodenuding occurs in air (i.e. oxidizing environment). Thus, while at low temperature (<300 ^{0}C), thermodenuding will be less likely to char, the particles may be more susceptible to oxidation due to an oxidizing environment. Oxidation of refractory carbon soot typically occurs at significantly elevated temperatures, but can occur at lower temperatures as well, especially if catalyzed due to impurities in the soot (Stanmore et al., 2001). Soot oxidation is likely limited in thermodenuding due to the low temperatures and relatively short residence time, but this issue will require more study in the future.

We finally discuss the assumption 4), which is the focus of our study. Previous studies have shown that nascent soot particles can restructure during the condensation or evaporation of the coating material depending on their surface tension (e.g., Ebert et al., 2002; Ma et al., 2013; Tritscher et al., 2011). Xue et al. (2009) found significant restructuring of soot particles when the particles were first coated with glutaric acid and then denuded. Ghazi and Olfert (2013) reported the dependence of soot restructuring on the mass amount of different coating material types. This restructure alone can affect the soot particles optical properties. For example, a laboratory study was performed on soot compacted upon humidification; the study measured modest changes in the absorption cross section (5% to 14%) but the extinction cross section was much more sensitive to compaction, with changes of more than 30% (Radney et al., 2014). Similarly, China et al. (2015a) and China et al. (2015b) using numerical simulations, predicted small changes in the absorption cross section (a few percent), but a much more substantial change in the total scattering cross section (up to ~300%), upon soot compaction. In addition to affecting the optical properties, changes in the soot structure can also affect the results of laser induced incandescence measurements (Bambha et al., 2013a). Finally, the condensation of secondary organic matter preferentially takes place in empty pores on soot particles and therefore, it is possible that compaction might affect secondary organic condensation on soot (Popovicheva et al., 2003). Two potential explanations for the soot restructuring detected during these studies can be: 1) Soot might be compacted during condensation of the coating materials due to surface tension effects (Huang et al., 1994; Schnitzler et al., 2017; Tritscher et al., 2011; Zhang et al., 2008). 2) The removal of the coating material during the subsequent thermodenuding may cause compaction when the coating evaporates, still due to surface tension effects (Ebert et al., 2002; Ma et al., 2013). However, we hypothesize a third potential pathway for soot restructuring, in which restructuring might take place solely due to the thermodenuding process, through the added thermal energy. There are a few evidences that the thermodenuding process can favor the compaction of lacy aggregates, even in absence of

coating material that condensed onto the primary emitted aggregates. If a similar process happens for ambient soot that would potentially bias the measured properties (e.g., absorption or scattering enhancements) of soot when a thermodenuder is used. The main objective of our study is to test this hypothesis to assure that the themodenuding process alone does not introduce this bias. A couple of potential restructuring processes, induced while thermodenuding aggregates, are discussed next:

a) When heated, fractal-like aggregates of metal nanoparticles, such as silver, copper and metallic oxides (e.g., titania), have been found to restructure to more compact morphologies at temperatures well below the bulk material melting points. For example, thermal restructuring has been found in silver aggregates, even at temperatures as low as 100 ºC, with full compaction at just 350 ºC (much below the melting temperature of silver), while the primary particle size remained unchanged (Weber et al., 1996; Weber and Friedlander, 1997). Another study found that aggregates of titania started to collapse when temperatures reached 700 ºC (Jang and Friedlander, 1998). These authors speculated that the heating causes the weakest branches in an aggregate to rotate around their contact points, resulting in the aggregate restructuring. Alternatively, Schmidt-Ott (1988) hypothesized that the monomers in silver nanoparticles aggregates might slide on each other when heated, also causing compaction. Both processes would restructure the aggregates without complete breakage of the bonds between the monomers due to Van der Waals forces.

b) As mentioned earlier, nascent soot aggregates typically have polycyclic aromatic hydrocarbons thinly coating them. This nascent coating could play a role in determining the soot structure if the coating properties (i.e., viscosity and surface tension) change at the higher temperature of the thermodenuder. Chen et al. (2016) found that some polycyclic aromatic hydrocarbons like phenanthrene and flouranthene, when present as a subnanometer layer on soot, behaved as subcooled liquid that weakened the bonds between the monomers, allowing them to slide and roll over each other and resulting in soot restructuring. Rothenbacher et al. (2008) provided some evidences that thermodenuding might make a difference in the strength of the adhesive bonds between the monomers. For aged soot, they found that a higher degree of fragmentation was seen for thermodenuded particles (75% at 280 ºC) than for untreated particles (60%) when impacted at ~ 200 m/s. The degree of fragmentation was defined as the fraction of broken bonds in an aggregate. Although, the process involved both the effect of coating and impaction, the higher degree of fragmentation for thermodenuded particles suggests that the thermal energy has a role on the increased degree of fragmentation.

These evidences motivated us to study potential effects on the specific case of nascent soot. With this goal in mind, we analyze the structure of laboratory generated nascent soot particles produced from two different fuel sources (ethylene flame and methane flame) and size selected at different mobility diameters before and after thermodenuding. This assessment is important for evaluating the potential biases that might be introduced by thermodenuding while, for example, estimating the absorption or scattering enhancements of laboratory or ambient soot particles.

2 Experiment

2.1 Experimental setup and sample collection

We analyzed five pairs of mobility-selected soot samples collected during two different experiments: the Boston College Experiment 2 (BC2) and the Boston College Experiment 4 (BC4). The sampling schematics are shown in the Figure 1a and b. None of the samples were coated with additional external coating material and the minimal coating present on the nascent soot was solely due to fuel residuals accumulated during the combustion and dilution processes.

Three soot sample sets were collected during BC2 from the combustion of ethylene and oxygen using a premixed flat flame burner (Cross et al., 2010). The fuel equivalence ratio (∅) for all the three sample sets was 2.1. A TD (Huffman et al., 2008) was used to remove volatile components from the nascent soot particles. The heating section of the TD was set at 250 °C to vaporize the non-refractory soot components which were absorbed by a charcoal section maintained at room temperature. Particles for a range of mobility diameters (d_m) were selected to investigate the effect of thermodenuding on particle size. Since the soot particles were only minimally coated, the thermodenuded particles had only slightly smaller mobility diameter than the initial particles. For our investigation, we selected three sets of nascent vs. nascent-denuded soot particles with d_m = 153 nm, 181 nm and 250 nm for nascent soot particles and d_m = 151 nm, 175 nm and 241 nm for the corresponding denuded soot particles. Soot particles were collected on 13 mm diameter Nuclepore polycarbonate filters having a pore size of 0.3 μm (Whatman Inc, Chicago, Illinois, USA). Additional details of the BC2 experimental set-up are provided elsewhere (Cross et al., 2010).

In addition, we selected two sets of soot samples generated during BC4 from the combustion of methane in an inverted diffusion flame burner (methane and O_2 mixture) at a d_m of 250 nm. The ∅ for both sample sets was about 0.7. As in BC2, a Huffman TD (heating section set at 270 °C) was used to remove the volatile components. For both experiments, the sample flow rate through the TD was 2 LPM resulting in a residence time of 5s in the heating section and 4s in the denuder section. During BC4, unlike during BC2, particles were first mobility size selected by a Differential Mobility Analyzer (DMA, TSI Inc.) and mass selected by a Centrifugal Particle Mass Analyzer (CPMA, Cambustion Ltd.) before thermodenuding. The first set of samples consisted of nascent and nascent-denuded soot, while the second set consisted of nascent-oxidized and nascent-oxidized-denuded soot. Soot was oxidized by exposure to ozone and hydroxyl radicals in a Potential Aerosol Mass (PAM) oxidation flow reactor (Lambe et al., 2011) and the nascent-oxidized soot was thermo-denuded at a temperature of 270 °C. The set of nascent-oxidized soot samples was included here to investigate if the thermodenuding effect is different for nascent versus nascent-oxidized soot. During BC4, soot particles were collected on 13 mm diameter Nuclepore filters having a pore size of 0.1 μm diameter (Whatman Inc, Chicago, Illinois, USA).

All the filters were coated with 1.8 nm thick layer of Pt/Pd alloy in a sputter coater (Hummer® 6.2) and imaged with a Hitachi S-4700 field emission scanning electron microscope (FE-SEM). From the FE-SEM images, several morphological parameters were evaluated (China et al 2014) using the image processing software ImageJ (Schneider et al., 2012).

2.2 Soot morphological parameters

Soot particles are aggregates of monomers that exhibit scale-invariant fractal structures (Forrest and Witten Jr, 1979; Sorensen et al., 1992). Soot aggregates can therefore be characterized by a fractal dimension *(D_f)* in which the mass of the aggregate *M* (proportional to the number of monomers *N* in the aggregate) scales with the ratio of the radius of gyration *(R_g)* to the radius of the monomers *(R_p),* as in M (or N) $\propto (R_g/R_p)^{D_f}$ (Klein and Meakin, 1989). To quantify the soot morphology, D_f is a commonly used parameter. Lacy soot particles have low D_f values, while compact soot particles have higher D_f values. The D_f of an ensemble of soot particles can be calculated by plotting N vs. R_g (or a surrogate for it). N scales with R_g as a power law with exponent D_f (Köylü et al., 1995b):

$$N = k_g \left(\frac{R_g}{R_p}\right)^{D_f} \quad (1)$$

where k_g is a pre-factor whose value depends on the overlap between the monomers in the aggregate. The relation formulated by Köylü et al. (1995a) was used to estimate D_f with geometric mean diameter *($\sqrt{LW}$)* of aggregate as a surrogate for $2R_g$:

$$N = k_{LW} \left(\frac{\sqrt{LW}}{2R_p}\right)^{D_f} \quad (2)$$

where L is the maximum length and W is the maximum width (orthogonal to L), K_{LW} is a prefactor and R_p is calculated from the mean of the projected area of the monomer. In general, it is difficult to measure N using an SEM image alone, because only two-dimensional (2-D) projections of the soot particles are typically available. Therefore, N is often estimated from the projected area of the soot aggregate A_p and the mean projected area of the monomers A_m using the relation provided by Oh and Sorensen (1997):

$$N = k_a \left(\frac{A_p}{A_m}\right)^{\alpha} \quad (3)$$

where α and k_a are constants that depend on the overlap between monomers in the 2-D projected image of the particle. In our case, we used K_a = 1.15 and α= 1.09 for all our nascent and nascent-denuded soot aggregates (Köylü et al., 1995b). This selection of K_a and α values is reasonable since we only studied nascent soot particles that are minimally coated.

In addition to D_f, several other 2-D morphological parameters were calculated from the FE-SEM images to investigate potential changes due to thermodenuding. The calculated parameters included roundness, convexity, aspect ratio (*AR)* and area equivalent diameter *(D_{Aeq})*. Figure 2a shows the definition of some of these parameters. D_{Aeq} is the diameter of a spherical particle with a projected area equivalent to the projected area of the aggregate. Roundness is calculated from the ratio of the projected area of the aggregate to the area of the circle having a diameter equal to the maximum projected length L and fully inscribing the projected image of the aggregate (Fig. 2b). Convexity (sometimes termed solidity) is the ratio of the projected area of the particle to the area of the smallest convex hull polygon, in which the 2-D projection of the aggregate is inscribed (Fig. 2c). AR is calculated as the ratio of L to W. Higher values of roundness and convexity or lower AR often correspond to more compact soot particles. In total, 1224 images of individual soot particles were analyzed.

3 Results and discussion

We analyzed images from four sets of nascent and nascent-denuded soot sample pairs of different sizes and a fifth set of nascent-oxidized denuded soot. Examples of images of soot particles before and after thermodenuding are shown in Fig. 3.

N1, N2, N3 and *N4* are 4 differently sized nascent soot particles and *D1, D2, D3* and *D4* are the corresponding nascent-denuded sets. *N5-D5* is a pair of nascent-oxidized soot before and after thermodenuding. Table1 summarizes the features of the analyzed soot particles. Sets *N1-D1, N2-D2* and *N3-D3* are the three sets from BC2 while sets *N4-D4* and *N5-D5* are from BC4.

In Table 1, for fuel type, E = ethylene and M = methane. N is the average number of monomers per aggregate estimated in each sample using Eq. (3). K_g values have been estimated using the relation $K_g = K_{L \cdot W} (1.17)^{Df}$ where $\sqrt{LW}/2R_g = 1.17$ has been taken from (Köylü et al., 1995b) and the values of $K_{L \cdot W}$ and D_f have been calculated from a log-log plot using Eq. (2). d_m is the mean mobility diameter (in nm) and M_{CPMA} represents the mean mass of the particle (in fg) as measured by the CPMA. For D_f, the term in parenthesis is the standard error calculated from the power fit using Eq. (2).

The largest decrease in the mean value of d_p (by 5.6 %) after thermodenuding is found for the *N3-D3* set. The decrease in d_p could be due to the partial removal of material volatile at the TD temperature and present on the nascent soot. The decrease in the monomer size after thermal treatment was previously observed when soot samples were heated at higher temperatures (from 400 ºC to 900 ºC) due to the removal of part of the nascent PAH layer from the monomers surface (Raj et al., 2014). Also, the mean value of d_p is smaller for the inverted diffusion flame when particles are sampled at the same mobility diameter of 250 nm. This suggests that there was less volatile material present in nascent soot generated from the inverted flame. This could be due to the different type of fuel as well as $\emptyset$. For the inverted diffusion flame of methane, $\emptyset$ was set at a lower value of ~ 0.7 compared to 2.1 for the pre-mixed flat flame of ethylene. For soot generated by an inverted diffusion flame, Ghazi and Olfert (2013), found no measurable amount of volatile material when the mass was measured by a CPMA before and after thermodenuding while for the nascent soot containing 0.1 mass fraction of non-refractory material (at $\emptyset$ =2.1) from an ethylene flat flame, Slowik et al. (2007) found that thermodenuding removed only about 0.05 mass fraction of volatile material.

To investigate whether the soot aggregate restructured after thermal denuding, we first analyze the changes in D_f as summarized in Fig. 4. For all the five sample sets, D_f lies between 1.65 and 1.86 (Table 1). These values of D_f are in agreement with observations made in previous studies on nascent soot particles produced from different fuel sources e.g., (Dhaubhadel et al., 2006; Sorensen, 2001). Also for all nascent vs. denuded pairs (except for the nascent-oxidized pair: *N5-D5*), there is no significant change (within 1σ) in D_f after thermodenuding (Fig. 4). For the *N5-D5* pair, D_f changes by about 9% (from 1.65 to 1.80) whereas for all other cases, the change is less than 2.3 %. The CPMA data for BC4 sample shows that the mass decreased from 2.37 to 2.34 fg for nascent soot, while for the nascent-oxidized

soot of the same mobility size, the mass decreased from 2.41 to 2.18 fg after thermodenuding. The larger decrease in mass for the nascent oxidized soot suggests that coating material on the oxidized soot was removed during thermodenuding. A possible explanation for the increase of D_f after thermodenuding the oxidized soot might be that the soot structure was slightly modified during the evaporation of the coating material. Interestingly, for the BC2 soot samples, there is no significant change in D_f despite the remarkable change in mass (~ 25%) of soot after thermodenuding (see CPMA data in Table 1). This result suggests that for BC2 sample sets, the removal of coating present on nascent soot does not affect the structure of soot. This is most probably due to the chemical composition of organics that were removed by TD. Cross et al. (2010) observed only minor restructuring of soot when dioctyl sebacate coating was removed by thermodenuding, suggesting that the removal of aliphatic compound may have little impact on the restructuring of soot. For soot from a flat flame burner, Slowik et al. (2004) found that the OC content (mass fraction of 0.1) was composed of comparable amount of aliphatic and aromatic compounds at lower ϕ (ϕ= 1.85) but at higher ϕ (ϕ>4), the OC content (mass fraction of 0.55) had only minor fraction of aliphatic compounds. We thus hypothesize that the nascent organics on the soot from the BC2 experiments considered here consisted in large fraction of aliphatic compounds.

To further investigate possible morphological changes after thermodenuding, we studied the convexity and roundness of soot particles for all five sample sets. The maximum change in the mean value of roundness occurs for set *N3-D3* (about 18%) and followed by the set *N4-D4* (about 13%). For the other sets, the mean value of roundness changes by less than 10%. For the case of convexity, the maximum change in the mean value occurs for set *N4-D4* (about 8%). For all other sets, the mean value of convexity changes by less than 5%.

In Fig. 5a and 5b we show box and whisker plots for the convexity and the roundness, respectively of the soot particles before and after thermodenuding. The convexity ranges from 0.37 to 0.91, while the roundness ranges from 0.09 to 0.75 (see Table 1 for details). No substantial changes in roundness or convexity are evident after thermodenuding.

In Fig. 6, we show probability distributions of convexity and roundness for all nascent and denuded soot pairs. The solid and the dashed lines represent the mean values for nascent and denuded soot respectively, while the shaded color bands in blue and orange represent one standard deviation. These means and uncertainty bands are calculated with a bootstrap approach, resampling with replacement from the raw data and constructing 100,000 frequency distributions (Wilks, 2011).

For four of the five sets, we observe minor changes in convexity and roundness. For the *N3-D3* pair, the distribution of convexity and roundness peaks at slightly lower values after thermodenuding. The convexity of particles decreases slightly with increasing value of the mobility diameter for both nascent and denuded particles. This suggests that smaller soot particles are more compact compared to larger particles, in agreement with previous studies (Chakrabarty et al., 2006; Virtanen et al., 2004). Figure 6a also suggests that for smaller mobility diameters, the convexity of soot from the ethylene diffusion flame might be less affected by thermodenuding compared to the larger sized particles.

With the methane diffusion flame (*N4-D4* and *N5-D5* sets), particles showed a negligible change in convexity after thermodenuding for both nascent and nascent-oxidized soot (Fig. 6a *N4-D4* and *N5-D5* respectively).

For completeness, we also investigated the changes in AR and D_{Aeq}, both show only small changes after thermodenuding (Table 1). Our observations on the 5 sets of soot pairs show that the morphology of nascent soot does not change significantly after thermodenuding. Exceptions are the roundness for *N3-D3* and *N4-D4* sets and the convexity for *N4-D4* pairs, which showed some statistically significant, but still small changes. Roundness and convexity on nascent-oxidized soot pair (*N5-D5*) showed no significant change after thermodenuding. However, the change in D_f (1.65±0.05 to 1.80 ±0.05) is significant. Since we have only a single set for the nascent-oxidized soot, we are unable to draw with confidence a conclusion on the effect of thermodenuding on such particles. However, the changes in D_f suggest that the different nanophysical properties of the nascent-oxidized soot might indeed result in a higher sensitivity to thermodenuding. In a study on the fragmentation and bond strength of diesel soot, Rothenbacher et al. (2008) made a comparison between nascent soot treated with and without a TD as a function of impact velocity and found no substantial change in the degree of fragmentation of nascent soot aggregates due to the thermodenuding. A low-pressure impactor was used to impart velocities up to 300m/s to the soot particles. The TD used in their study had a residence time of 0.43 s and the sample was heated to 280 ºC. In another study by Raj et al. (2014), soot fragmentation was observed after thermodenuding in the temperature range of 400-900 ºC on diesel soot and commercial soot (Printex-U). However, in the lower temperature range, below 500 ºC, they found a minor effect on soot fragmentation. Bambha et al. (2013b) noticed little effect of thermodenuding at 410 ºC (transit time of ~34 s) on the morphology of soot during the removal of oleic acid coating. In another study, Slowik et al. (2007) did not observe any measurable change in the structure of soot when fresh soot (generated at $\emptyset$ = 2.1 and 3.5) was thermodenuded at 200 ºC. Our results of the negligible or minor restructuring of thermodenuded soot particles are in agreement with these previous studies suggesting that these results are robust and reproducible. Although, in past studies thermodenuding showed appreciable effects on the structure of metal aggregates like silver, we did not observe such effect for nascent soot aggregates when heated up to 270 ºC.

4 Summary

In this study, we used scanning electron microscopy to investigate the morphology of nascent soot aggregates prior and after thermodenuding in a low-temperature regime (< 270 ºC). Despite mass losses up to ~29% in the nascent soot, only minor effects on the soot structure were detected after thermodenuding, irrespective of the fuel type. No significant change in D_f was observed; the only exception was the fractal dimension of nascent-oxidized soot, although roundness and convexity showed only minor changes also in this case. Future work should focus on the effect of higher thermodenuding temperatures to investigate temperature effects on the structure of nascent soot.

The image analysis data used in this paper are publicly available on the Digital Commons repository of Michigan Technological University and can be found here: http://digitalcommons.mtu.edu/physics-fp/80

Acknowledgements

This work was supported in part by the Office of Science (BER), Department of Energy (Atmospheric System Research) Grant no. DE-SC0011935 and no. DE-SC0010019, and Atmospheric Chemistry program of the National Science Foundation Grant no. AGS-1536939 to Boston College, 1537446 to Aerodyne Research Inc. S. China was partially supported by a NASA Earth and Space Science Graduate Fellowships no. NNX12AN97H.

References

Adachi, K. and Buseck, P.: Internally mixed soot, sulfates, and organic matter in aerosol particles from Mexico City, Atmospheric Chemistry and Physics, 8, 6469-6481, 2008.

Adachi, K. and Buseck, P. R.: Changes of ns-soot mixing states and shapes in an urban area during CalNex, Journal of Geophysical Research: Atmospheres, 118, 3723-3730, 2013.

Bambha, R., Dansson, M. A., Schrader, P. E., and Michelsen, H. A.: Effects of volatile coatings on the morphology and optical detection of combustion-generated black carbon particles, Sandia National Laboratories (SNL-CA), Livermore, CA (United States), 2013a.

Bambha, R. P., Dansson, M. A., Schrader, P. E., and Michelsen, H. A.: Effects of volatile coatings and coating removal mechanisms on the morphology of graphitic soot, Carbon, 61, 80-96, 2013b.

Buseck, P. R., Adachi, K., Gelencsér, A., Tompa, É., and Pósfai, M.: Ns-soot: a material-based term for strongly light-absorbing carbonaceous particles, Aerosol Science and Technology, 48, 777-788, 2014.

Cappa, C. D., Onasch, T. B., Massoli, P., Worsnop, D. R., Bates, T. S., Cross, E. S., Davidovits, P., Hakala, J., Hayden, K. L., and Jobson, B. T.: Radiative absorption enhancements due to the mixing state of atmospheric black carbon, Science, 337, 1078-1081, 2012.

Cappa, C. D., Onasch, T. B., Massoli, P., Worsnop, D. R., Bates, T. S., Cross, E. S., Davidovits, P., Hakala, J., Hayden, K. L., and Jobson, B. T.: Response to Comment on" Radiative Absorption Enhancements Due to the Mixing State of Atmospheric Black Carbon", Science, 339, 393-393, 2013.

Chakrabarty, R. K., Moosmüller, H., Arnott, W. P., Garro, M. A., and Walker, J.: Structural and fractal properties of particles emitted from spark ignition engines, Environmental science & technology, 40, 6647-6654, 2006.

Chen, C., Fan, X., Shaltout, T., Qiu, C., Ma, Y., Goldman, A., and Khalizov, A. F.: An unexpected restructuring of combustion soot aggregates by subnanometer coatings of polycyclic aromatic hydrocarbons, Geophysical Research Letters, 43, 2016.

Cheng, Y., Duan, F.-k., He, K.-b., Zheng, M., Du, Z.-y., Ma, Y.-l., and Tan, J.-h.: Intercomparison of thermal–optical methods for the determination of organic and elemental carbon: influences of aerosol composition and implications, Environmental science & technology, 45, 10117-10123, 2011.

China, S., Kulkarni, G., Scarnato, B. V., Sharma, N., Pekour, M., Shilling, J. E., Wilson, J., Zelenyuk, A., Chand, D., and Liu, S.: Morphology of diesel soot residuals from supercooled water droplets and ice crystals: implications for optical properties, Environmental Research Letters, 10, 114010, 2015a.

China, S., Salvadori, N., and Mazzoleni, C.: Effect of traffic and driving characteristics on morphology of atmospheric soot particles at freeway on-ramps, Environmental science & technology, 48, 3128-3135, 2014.

China, S., Scarnato, B., Owen, R. C., Zhang, B., Ampadu, M. T., Kumar, S., Dzepina, K., Dziobak, M. P., Fialho, P., and Perlinger, J. A.: Morphology and Mixing State of Aged Soot Particles at a Remote Marine Free Troposphere Site: Implications for Optical Properties, Geophysical Research Letters, 2015b. 2015b.

Chow, J. C., Watson, J. G., Chen, L.-W. A., Arnott, W. P., Moosmüller, H., and Fung, K.: Equivalence of elemental carbon by thermal/optical reflectance and transmittance with different temperature protocols, Environmental science & technology, 38, 4414-4422, 2004.

Countess, R. J.: Interlaboratory analyses of carbonaceous aerosol samples, Aerosol Science and Technology, 12, 114-121, 1990.

Cross, E. S., Onasch, T. B., Ahern, A., Wrobel, W., Slowik, J. G., Olfert, J., Lack, D. A., Massoli, P., Cappa, C. D., and Schwarz, J. P.: Soot particle studies—instrument inter-comparison—project overview, Aerosol Science and Technology, 44, 592-611, 2010.

Dhaubhadel, R., Pierce, F., Chakrabarti, A., and Sorensen, C.: Hybrid superaggregate morphology as a result of aggregation in a cluster-dense aerosol, Physical Review E, 73, 011404, 2006.

Ebert, M., Inerle-Hof, M., and Weinbruch, S.: Environmental scanning electron microscopy as a new technique to determine the hygroscopic behaviour of individual aerosol particles, Atmospheric Environment, 36, 5909-5916, 2002.

Forrest, S. and Witten Jr, T.: Long-range correlations in smoke-particle aggregates, Journal of Physics A: Mathematical and General, 12, L109, 1979.

Fuller, K. A., Malm, W. C., and Kreidenweis, S. M.: Effects of mixing on extinction by carbonaceous particles, Journal of Geophysical Research: Atmospheres (1984–2012), 104, 15941-15954, 1999.

Ghazi, R. and Olfert, J.: Coating mass dependence of soot aggregate restructuring due to coatings of oleic acid and dioctyl sebacate, Aerosol Science and Technology, 47, 192-200, 2013.

Haynes, B. S. and Wagner, H. G.: Soot formation, Progress in Energy and Combustion Science, 7, 229-273, 1981.
Healy, R., Wang, J., Jeong, C. H., Lee, A., Willis, M., Jaroudi, E., Zimmerman, N., Hilker, N., Murphy, M., and Eckhardt, S.: Light-absorbing properties of ambient black carbon and brown carbon from fossil fuel and biomass burning sources, Journal of Geophysical Research: Atmospheres, 120, 6619-6633, 2015.
Huang, P.-F., Turpin, B. J., Pipho, M. J., Kittelson, D. B., and McMurry, P. H.: Effects of water condensation and evaporation on diesel chain-agglomerate morphology, Journal of Aerosol Science, 25, 447-459, 1994.
Huffman, J. A., Ziemann, P. J., Jayne, J. T., Worsnop, D. R., and Jimenez, J. L.: Development and characterization of a fast-stepping/scanning thermodenuder for chemically-resolved aerosol volatility measurements, Aerosol Science and Technology, 42, 395-407, 2008.
Jacobson, M. Z.: Strong radiative heating due to the mixing state of black carbon in atmospheric aerosols, Nature, 409, 695-697, 2001.
Jang, H. D. and Friedlander, S. K.: Restructuring of chain aggregates of titania nanoparticles in the gas phase, Aerosol Science and Technology, 29, 81-91, 1998.
Khalizov, A. F., Lin, Y., Qiu, C., Guo, S., Collins, D., and Zhang, R.: Role of OH-initiated oxidation of isoprene in aging of combustion soot, Environmental science & technology, 47, 2254-2263, 2013.
Khalizov, A. F., Xue, H., Wang, L., Zheng, J., and Zhang, R.: Enhanced light absorption and scattering by carbon soot aerosol internally mixed with sulfuric acid, The Journal of Physical Chemistry A, 113, 1066-1074, 2009.
Khan, B., Hays, M. D., Geron, C., and Jetter, J.: Differences in the OC/EC ratios that characterize ambient and source aerosols due to thermal-optical analysis, Aerosol Science and Technology, 46, 127-137, 2012.
Klein, R. and Meakin, P.: Universality in colloid aggregation, Nature, 339, 1989.
Knox, A., Evans, G., Brook, J., Yao, X., Jeong, C.-H., Godri, K., Sabaliauskas, K., and Slowik, J.: Mass absorption cross-section of ambient black carbon aerosol in relation to chemical age, Aerosol Science and Technology, 43, 522-532, 2009.
Köylü, Ü. Ö., Faeth, G., Farias, T. L., and Carvalho, M. d. G.: Combustion and Flame, 100, 621-633, 1995a.
Köylü, Ü. Ö., Faeth, G., Farias, T. L., and Carvalho, M. d. G.: Fractal and projected structure properties of soot aggregates, Combustion and Flame, 100, 621-633, 1995b.
Lack, D. and Cappa, C.: Impact of brown and clear carbon on light absorption enhancement, single scatter albedo and absorption wavelength dependence of black carbon, Atmospheric Chemistry and Physics, 10, 4207-4220, 2010.
Lack, D. A., Langridge, J. M., Bahreini, R., Cappa, C. D., Middlebrook, A. M., and Schwarz, J. P.: Brown carbon and internal mixing in biomass burning particles, Proceedings of the National Academy of Sciences, 109, 14802-14807, 2012.
Lambe, A., Ahern, A., Williams, L., Slowik, J., Wong, J., Abbatt, J., Brune, W., Ng, N., Wright, J., and Croasdale, D.: Characterization of aerosol photooxidation flow reactors: heterogeneous oxidation, secondary organic aerosol formation and cloud condensation nuclei activity measurements, Atmospheric Measurement Techniques, 4, 445-461, 2011.
Liu, D., Taylor, J. W., Young, D. E., Flynn, M. J., Coe, H., and Allan, J. D.: The effect of complex black carbon microphysics on the determination of the optical properties of brown carbon, Geophysical Research Letters, 2015a. 2015a.
Liu, S., Aiken, A. C., Gorkowski, K., Dubey, M. K., Cappa, C. D., Williams, L. R., Herndon, S. C., Massoli, P., Fortner, E. C., and Chhabra, P. S.: Enhanced light absorption by mixed source black and brown carbon particles in UK winter, Nature communications, 6, 2015b.
Ma, X., Zangmeister, C. D., Gigault, J., Mulholland, G. W., and Zachariah, M. R.: Soot aggregate restructuring during water processing, Journal of Aerosol Science, 66, 209-219, 2013.
Oh, C. and Sorensen, C.: The effect of overlap between monomers on the determination of fractal cluster morphology, Journal of colloid and interface science, 193, 17-25, 1997.
Park, K., Kittelson, D. B., and McMurry, P. H.: Structural properties of diesel exhaust particles measured by transmission electron microscopy (TEM): Relationships to particle mass and mobility, Aerosol Science and Technology, 38, 881-889, 2004.
Popovicheva, O., Persiantseva, N., Kuznetsov, B., Rakhmanova, T., Shonija, N., Suzanne, J., and Ferry, D.: Microstructure and water adsorbability of aircraft combustor soots and kerosene flame soots: toward an aircraft-generated soot laboratory surrogate, The Journal of Physical Chemistry A, 107, 10046-10054, 2003.
Radney, J. G., You, R., Ma, X., Conny, J. M., Zachariah, M. R., Hodges, J. T., and Zangmeister, C. D.: Dependence of soot optical properties on particle morphology: measurements and model comparisons, Environmental science & technology, 48, 3169-3176, 2014.
Raj, A., Tayouo, R., Cha, D., Li, L., Ismail, M. A., and Chung, S. H.: Thermal fragmentation and deactivation of combustion-generated soot particles, Combustion and Flame, 161, 2446-2457, 2014.
Rothenbacher, S., Messerer, A., and Kasper, G.: Fragmentation and bond strength of airborne diesel soot agglomerates, Particle and fibre toxicology, 5, 9, 2008.
Schmidt-Ott, A.: New approaches to in situ characterization of ultrafine agglomerates, Journal of Aerosol Science, 19, 553559-557563, 1988.
Schneider, C. A., Rasband, W. S., and Eliceiri, K. W.: NIH Image to ImageJ: 25 years of image analysis, Nature methods, 9, 671-675, 2012.
Schnitzler, E. G., Dutt, A., Charbonneau, A. M., Olfert, J. S., and Jäger, W.: Soot aggregate restructuring due to coatings of secondary organic aerosol derived from aromatic precursors, Environmental science & technology, 48, 14309-14316, 2014.
Schnitzler, E. G., Gac, J. M., and Jäger, W.: Coating surface tension dependence of soot aggregate restructuring, Journal of Aerosol Science, 106, 43-55, 2017.

Slowik, J. G., Cross, E. S., Han, J.-H., Kolucki, J., Davidovits, P., Williams, L. R., Onasch, T. B., Jayne, J. T., Kolb, C. E., and Worsnop, D. R.: Measurements of morphology changes of fractal soot particles using coating and denuding experiments: Implications for optical absorption and atmospheric lifetime, Aerosol science and technology, 41, 734-750, 2007.

Slowik, J. G., Stainken, K., Davidovits, P., Williams, L., Jayne, J., Kolb, C., Worsnop, D. R., Rudich, Y., DeCarlo, P. F., and Jimenez, J. L.: Particle morphology and density characterization by combined mobility and aerodynamic diameter measurements. Part 2: Application to combustion-generated soot aerosols as a function of fuel equivalence ratio, Aerosol Science and Technology, 38, 1206-1222, 2004.

Sorensen, C.: Light scattering by fractal aggregates: a review, Aerosol Science & Technology, 35, 648-687, 2001.

Sorensen, C., Cai, J., and Lu, N.: Light-scattering measurements of monomer size, monomers per aggregate, and fractal dimension for soot aggregates in flames, Applied Optics, 31, 6547-6557, 1992.

Stanmore, B. R., Brilhac, J.-F., and Gilot, P.: The oxidation of soot: a review of experiments, mechanisms and models, Carbon, 39, 2247-2268, 2001.

Swanson, J. and Kittelson, D.: Evaluation of thermal denuder and catalytic stripper methods for solid particle measurements, Journal of Aerosol Science, 41, 1113-1122, 2010.

Tritscher, T., Jurányi, Z., Martin, M., Chirico, R., Gysel, M., Heringa, M. F., DeCarlo, P. F., Sierau, B., Prévôt, A. S., and Weingartner, E.: Changes of hygroscopicity and morphology during ageing of diesel soot, Environmental Research Letters, 6, 034026, 2011.

Van Poppel, L. H., Friedrich, H., Spinsby, J., Chung, S. H., Seinfeld, J. H., and Buseck, P. R.: Electron tomography of nanoparticle clusters: Implications for atmospheric lifetimes and radiative forcing of soot, Geophysical Research Letters, 32, 2005.

Virtanen, A. K., Ristimäki, J. M., Vaaraslahti, K. M., and Keskinen, J.: Effect of engine load on diesel soot particles, Environmental science & technology, 38, 2551-2556, 2004.

Weber, A., Baltensperger, U., Gäggeler, H., and Schmidt-Ott, A.: In situ characterization and structure modification of agglomerated aerosol particles, Journal of aerosol science, 27, 915-929, 1996.

Weber, A. P. and Friedlander, S. K.: In situ determination of the activation energy for restructuring of nanometer aerosol agglomerates, Journal of Aerosol Science, 28, 179-192, 1997.

Wehner, B., Philippin, S., and Wiedensohler, A.: Design and calibration of a thermodenuder with an improved heating unit to measure the size-dependent volatile fraction of aerosol particles, Journal of aerosol science, 33, 1087-1093, 2002.

Westcott, S. L., Zhang, J., Shelton, R. K., Bruce, N. M., Gupta, S., Keen, S. L., Tillman, J. W., Wald, L. B., Strecker, B. N., Rosenberger, A. T., Davidson, R. R., Chen, W., Donovan, K. G., and Hryniewicz, J. V.: Broadband optical absorbance spectroscopy using a whispering gallery mode microsphere resonator, The Review of scientific instruments, 79, 033106, 2008.

Wilks, D. S.: Statistical methods in the atmospheric sciences, Academic press, 2011.

Xue, H., Khalizov, A. F., Wang, L., Zheng, J., and Zhang, R.: Effects of coating of dicarboxylic acids on the mass− mobility relationship of soot particles, Environmental science & technology, 43, 2787-2792, 2009.

Zhang, R., Khalizov, A. F., Pagels, J., Zhang, D., Xue, H., and McMurry, P. H.: Variability in morphology, hygroscopicity, and optical properties of soot aerosols during atmospheric processing, Proceedings of the National Academy of Sciences, 105, 10291-10296, 2008.

Table 1. Summary of physical and morphological parameters for the soot particles analyzed.

Experiment	**BC2**						**BC4**			
Sample	N1	D1	N2	D2	N3	D3	N4	D4	N5	D5
Fuel type	E	E	E	E	E	E	M	M	M	M
#Particles analyzed	108	151	113	163	114	109	113	105	122	125
N	41	55	121	104	110	153	158	188	155	166
d_m **(nm)**	153	151	181	175	250	241	250	250	250	250

M_{CPMA} **(fg)**	Mean	1.02	0.78	1.52	1.08	2.85	2.20	2.37	2.34	2.41	2.18
	S.D.	0.03	0.03	0.05	0.04	0.14	0.13	0.11	0.13	0.11	0.11
D_f	Mean	1.86	1.84	1.73	1.72	1.78	1.79	1.80	1.76	1.65	1.80
	S.E.	(0.05)	(0.04)	(0.05)	(0.06)	(0.08)	(0.05)	(0.05)	(0.06)	(0.05)	(0.05)
K_g	Mean	1.78	1.98	2.50	2.50	2.22	2.00	2.10	2.56	2.87	2.16
	S.E.	(0.04)	(0.03)	(0.05)	(0.05)	(0.08)	(0.06)	(0.06)	(0.07)	(0.06)	(0.06)
d_p **(nm)**	Mean	33.5	31.8	26.8	25.7	32.1	30.3	23.5	22.8	23.9	23.1
	Median	33.5	32.4	26.5	25.9	32.1	28.9	23.2	22.5	23.7	23.0
	S.D.	(2.1)	(3.3)	(2.7)	(2.6)	(2.1)	(6.9)	(3.1)	(2.2)	(2.5)	(3.4)
	S.E.	(0.21)	(0.27)	(0.26)	(0.21)	(0.20)	(0.66)	(0.30)	(0.22)	(0.23)	(0.31)
Roundness	Mean	0.41	0.43	0.36	0.34	0.38	0.31	0.31	0.35	0.33	0.33
	Median	0.42	0.42	0.35	0.35	0.35	0.30	0.30	0.34	0.32	0.31
	S.D.	(0.12)	(0.12)	(0.10)	(0.10)	(0.12)	(0.09)	(0.11)	(0.13)	(0.11)	(0.11)
	S.E.	(0.01)	(0.01)	(0.01)	(0.01)	(0.01)	(0.01)	(0.01)	(0.01)	(0.01)	(0.01)
Convexity	Mean	0.72	0.75	0.66	0.66	0.62	0.59	0.61	0.66	0.61	0.63
	Median	0.73	0.74	0.66	0.65	0.62	0.58	0.61	0.66	0.61	0.62
	S.D.	(0.09)	(0.09)	(0.09)	(0.10)	(0.09)	(0.10)	(0.10)	(0.11)	(0.12)	(0.11)
	S.E.	(0.01)	(0.01)	(0.01)	(0.01)	(0.01)	(0.01)	(0.01)	(0.01)	(0.01)	(0.01)
D_{Aeq} **(nm)**	Mean	169	181	220	196 189	255	262	215	230	219	214
	Median	171	175	208	(40)	262	260	199	220	213	202
	S.D.	(33)	(35)	(55)	(3)	(46)	(49)	(54)	(55)	(50)	(59)
	S.E.	(3)	(3)	(5)		(4)	(5)	(5)	(5)	(5)	(5)
AR	Mean	1.79	1.73	1.84	1.92	1.78	1.85	1.99	1.95	1.85	1.88
	Median	1.66	1.62	1.70	1.78	1.68	1.72	1.85	1.82	1.80	1.83
	S.D.	(0.51)	(0.42)	(0.49)	(0.51)	(0.57)	(0.50)	(0.60)	(0.60)	(0.50)	(0.50)
	S.E.	(0.05)	(0.03)	(0.05)	(0.04)	(0.05)	(0.05)	(0.06)	(0.06)	(0.05)	(0.04)

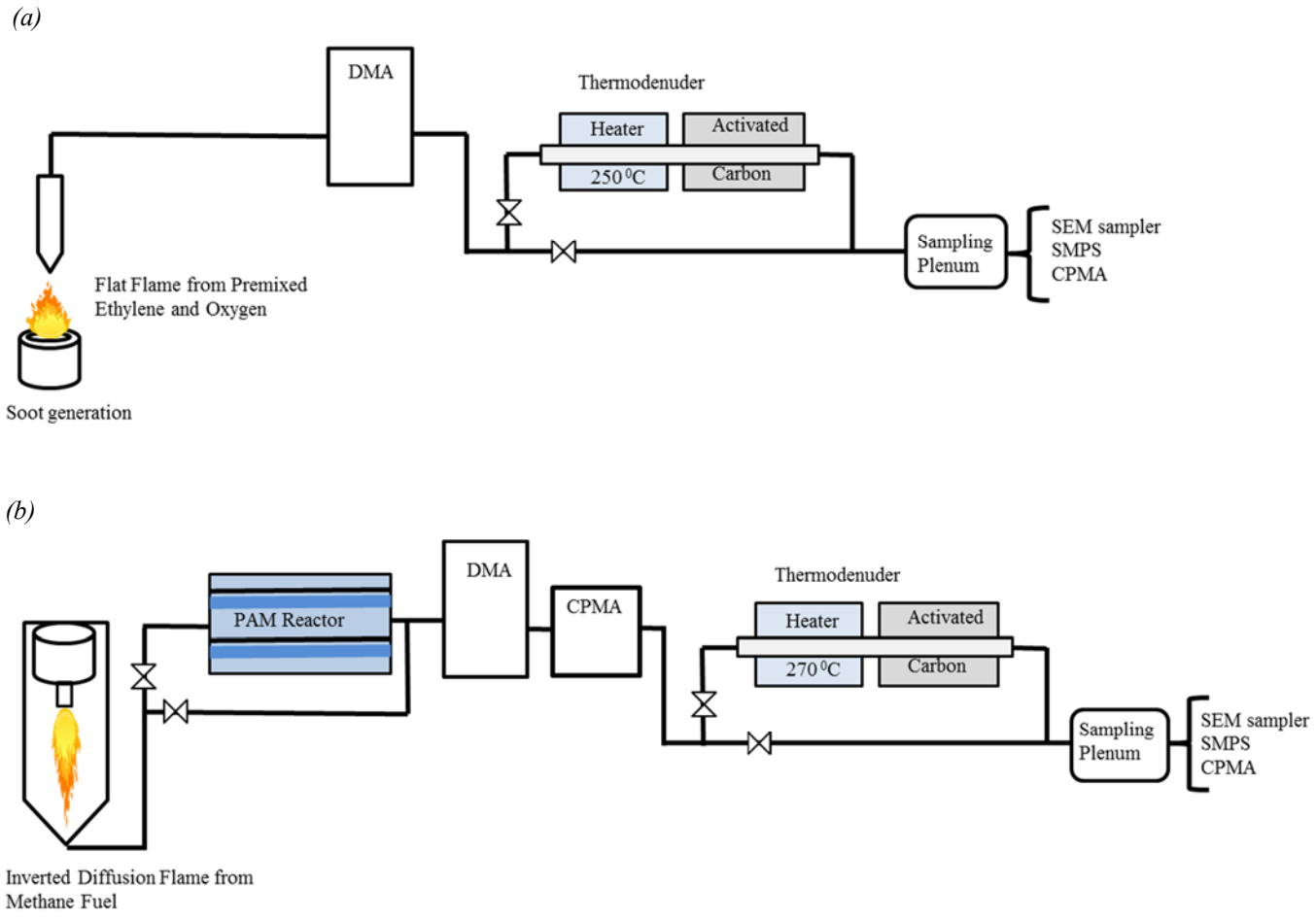

Figure. 1 (a) Soot generation and sampling in BC2. **(b)** Soot generation and sampling in BC4.

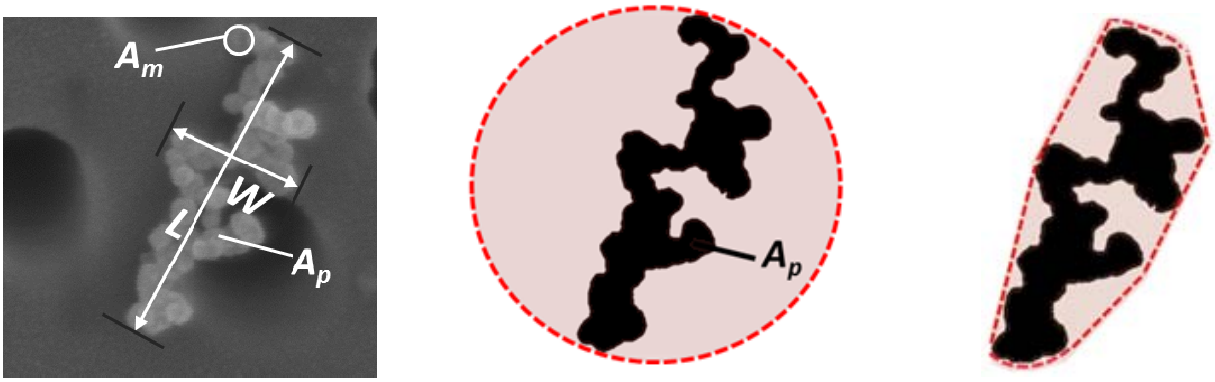

(a) *(b)* *(c)*

Figure 2. (a) Example of SEM image of a soot particle showing the definition of several parameters measured from the binary projected image: maximum projected length L, maximum projected width W, projected area of monomer A_m and projected area of particle A_p. **(b)** Schematic representation of the roundness calculation for the same soot

particle shown in (a). **(c)** Schematic representation of the convexity calculation for the same soot particle shown in (a). The pink shades in (b) and (c) represent the equivalent area for circle and convex hull, respectively, for the binary image of soot particle shown in (a).

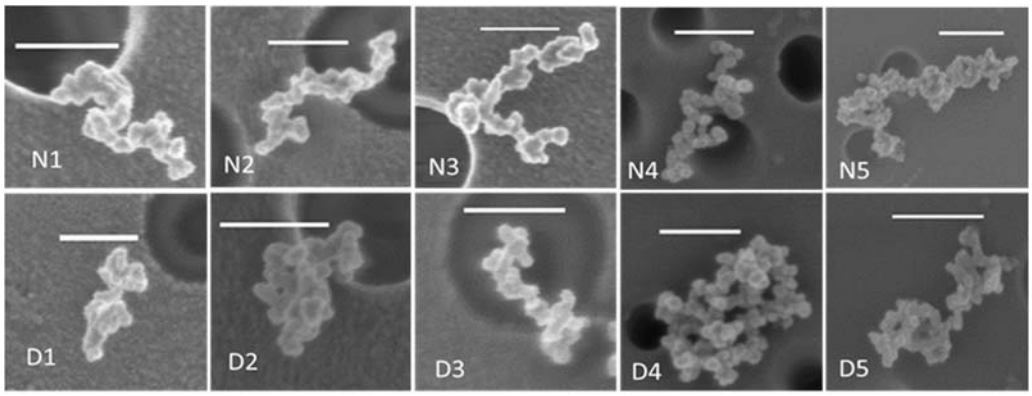

Figure 3. SEM micrographs of nascent (N) and thermodenuded (D) soot particles. The white horizontal bar in each micrograph represents a length scale of 200 nm.

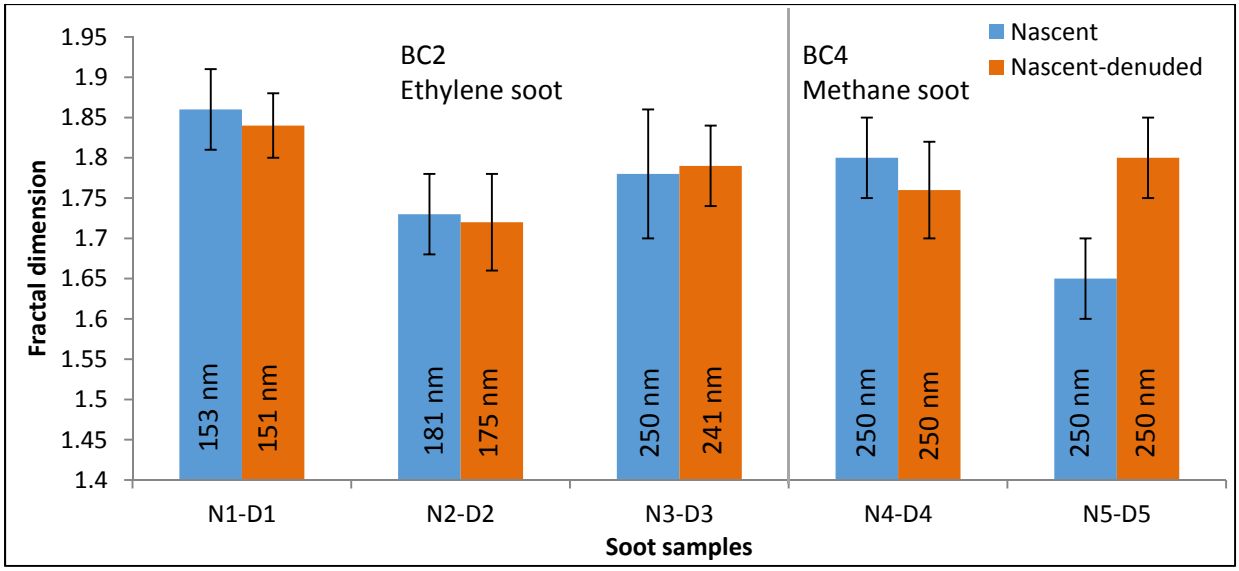

Figure 4. Fractal dimension of nascent (in blue) and nascent-denuded (in orange) soot pairs of different mobility sizes. The error bars represent the standard errors.

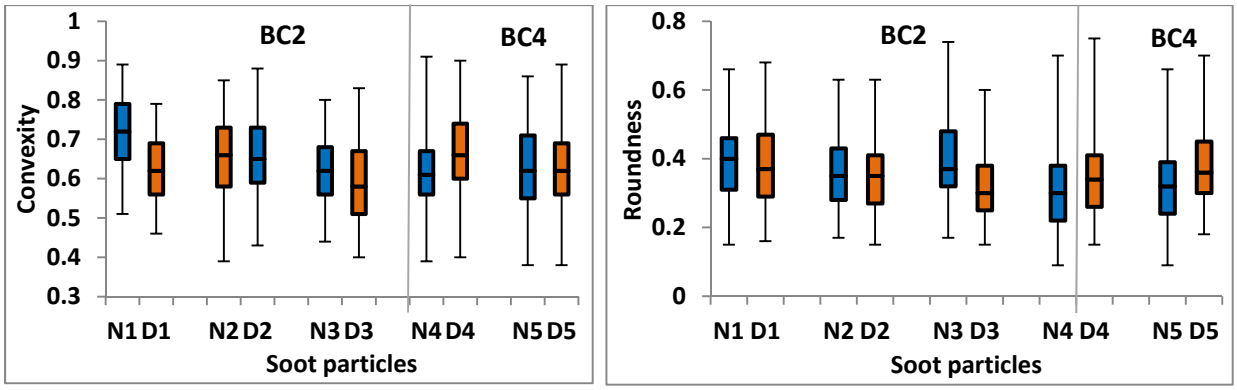

(a) *(b)*

Figure 5. Box and whisker plots of **a)** convexity and **b)** roundness. Blue boxes represent the nascent soot and orange boxes represent the nascent-denuded soot. The horizontal bar inside the box represents the median value while the lower part and upper part of the box separated by the horizontal bar represent the first and third quartiles respectively. The lower and upper extremities of the whiskers represent the minimum and maximum values, respectively.

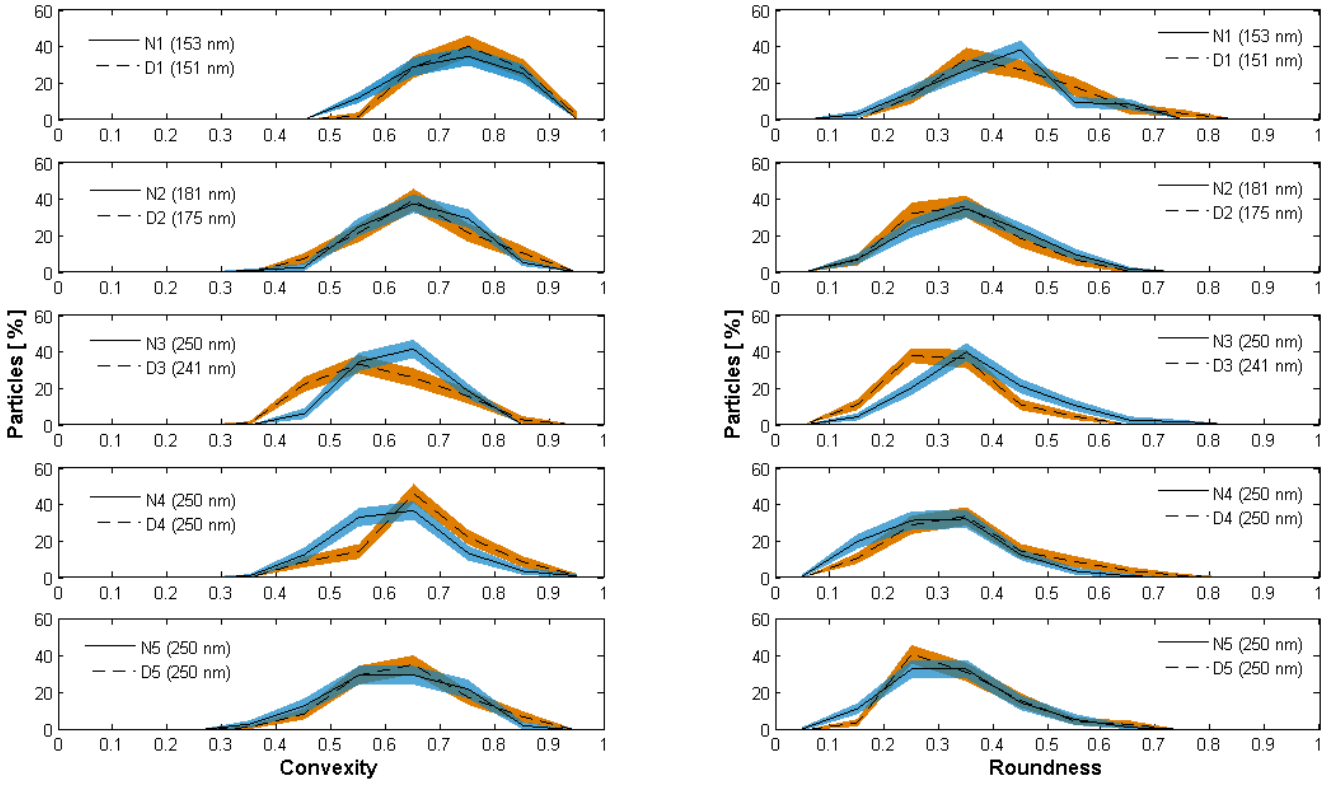

(a) *(b)*

Figure 6. Distributions of **a)** convexity and **b)** roundness for nascent and nascent-denuded soot particles of different sizes (the mobility diameter is reported in parenthesis in the legends).